APL Photonics

RESEARCH ARTICLE | JUNE 05 2026

Transfer-matrix modeling of spectral reflectivity for monitoring reactive-ion etching processes

A. P. Milenin ; J. R. Vaskasi; D. Kazakov ; Y. Shimura ; I. G. Koo ; F. Ferraro ; K. Devriendt

APL Photonics 11, 066104 (2026)
https://doi.org/10.1063/5.0314383

AIP Publishing

Transfer-matrix modeling of spectral reflectivity for monitoring reactive-ion etching processes

Cite as: APL Photon. 11, 066104 (2026); doi: 10.1063/5.0314383
Submitted: 28 November 2025 • Accepted: 18 May 2026 •
Published Online: 5 June 2026

A. P. Milenin,[a] J. R. Vaskasi, D. Kazakov, Y. Shimura, I. G. Koo, F. Ferraro, and K. Devriendt

AFFILIATIONS

IMEC, Kapeldreef 75, 3001 Heverlee, Belgium

[a]Author to whom correspondence should be addressed: Alexey.Milenin@imec.be

ABSTRACT

We apply the transfer matrix method (TMM) to model the evolution of light spectral reflectivity during reactive ion etching of SiGe heterostructures used in electro-absorption modulators. The simulated reflectivity as a function of etch depth shows excellent agreement with *in situ* light spectral reflectometry measurements, enabling identification of wavelength ranges most sensitive to changes in the quantum-well (QW) stack. For Ge-rich SiGe (~80% Ge), both modeling and experiment indicate a sensitivity window centered near 500 ± 50 nm, where the QW heterostructure exhibits a distinct spectral signature. We further show that introducing a thin SiGe etch-contrast layer (ECL) with ~10% Ge concentration offset from the strain-relaxed buffer composition produces a clear reflectivity response that simplifies end point determination. These results demonstrate how TMM-assisted wavelength selection and ECL engineering can enhance the robustness of etch end point algorithms for advanced SiGe photonic device fabrication.

I. INTRODUCTION

Precise control of etch depth is essential for achieving the target performance of SiGe electro-absorption modulators and other advanced photonic devices. Among process-monitoring approaches, *in situ* light spectral reflectometry (LSR) has become an effective method for real-time depth control during plasma etching, particularly when etching through optically distinct multilayer structures. Prior work has demonstrated the applicability of LSR for tracking wafer-to-wafer and lot-to-lot depth variability in shallow trench isolation (STI) processes using commercial tools, such as the LSR module of Lam Research.[1] However, modeling reflectivity signals in complex stacks during plasma etching, such as SiGe heterostructures used in quantum-confined Stark effect (QCSE) modulators, remains a thrilling task that is addressed in this publication.

To support process definition and end point strategy development, we combine experimental *in situ* reflectivity measurements with optical modeling based on the transfer matrix method (TMM). TMM is a well-established computational technique for evaluating light propagation and interference in multilayer stacks.[2] Several open-source implementations enable calculation of reflectivity and transmittance spectra using wavelength-dependent refractive indices and layer thicknesses.[3,4] Although it has not yet been reported, this approach should provide a predictive description of spectral evolution during etching, enabling direct comparison with experimentally acquired LSR data.

Reflectivity modeling to track etch-depth evolution during plasma etching has been previously reported.[5,6] In those as well as in other references on similar topics, the authors immediately attempt to model the reflectivity spectra of a patterned wafer, omitting in many cases the initial step of intensive characterization of the reflectivity spectra evolution during dry plasma etching for a complex stack without a lithography pattern. As it was mentioned in Ref. 5, the resulting reflectivity data of a patterned wafer is usually "very messy, and well suited to computer simulation." In this paper, we aim to address this gap by focusing on full spectral characterization of reflectivity evolution during a blanket film etching, which is done by utilizing the TMM technique that provides a fast, deterministic, and accurate solution for vertically stacked thin films, ideal for *in situ* monitoring of SiGe strain-relaxed buffer (SRB) etch-back application.

The SiGe QCSE modulator concept and its monolithic fabrication are described in Refs. 7 and 8. In the present work, however, a

different integration strategy is used, which involves wafer bonding of the modulator-containing epitaxial stack to a prefabricated silicon photonics substrate, followed by grinding and cleaning steps prior to plasma etching of the SiGe layers. A similar bonding-based integration strategy, although for III–V materials, is discussed, for example, in Ref. 9.

The first critical step is the removal of the SiGe SRB, typically 600–800 nm thick, while stopping precisely on a subsequent SiGe layer. Because this multilayer SiGe structure produces a well-defined reflectivity response during etching, SRB removal serves as an ideal test case for assessing the combined TMM–LSR approach. By modeling and experimentally validating the reflectivity evolution, we identify wavelength regions with high sensitivity to quantum well structure and sensitivity to etch-contrast layer (ECL), as well as the combination of wavelength for defining a tool-compatible end point algorithm without ECL.

II. EXPERIMENTAL AND MODELING PROCEDURE

A. Stack design, materials, and experimental setup

Multiple SiGe stacks with varying Ge concentrations were fabricated for modulator development. This study focuses on the Ge-rich stack (85% of Ge in the SiGe) shown in Fig. 1(a). The stack orientation inverts upon wafer bonding, see in Fig. 1(b), and both "as-grown" (direct) and "bonded" (flipped) stack configurations were characterized experimentally with corresponding TMM modeling of spectral reflectivity.

An etch-contrast layer of ~10% Ge content difference with respect to SRB was introduced in later iterations. Initial quantum-confined Stark effect (QCSE) stacks were grown without ECL, requiring precise etch stop on a heavily p-doped SiGe layer of identical Ge concentration to the SRB. Wafer-to-wafer (WtW) SRB thickness variability, arising from chemical–mechanical polishing (CMP) used between epitaxial growth steps, necessitates an end point detection method to stop the process when SRB is fully removed. While optical emission spectroscopy (OES) lacks sufficient sensitivity for this application, light spectral reflectometry provides a viable real-time monitoring approach that can be utilized for SRB removal.

In this study, the ECL thickness was set to 20 nm as a practical engineering trade-off for initial testing. While thinner layers could also be used based on the reflectometry sensitivity analysis presented later, a 20 nm thickness ensures a robust and clearly distinguishable reflectivity signature, enabling reliable estimation of the signal modulation amplitude under realistic conditions for the wavelength range of interest.

The process of SRB removal was defined in the Lam Research 2300® Kiyo®EX Series 300 mm conductor etch reactor, which contamination level allows the processing of bonded wafers. Several tests

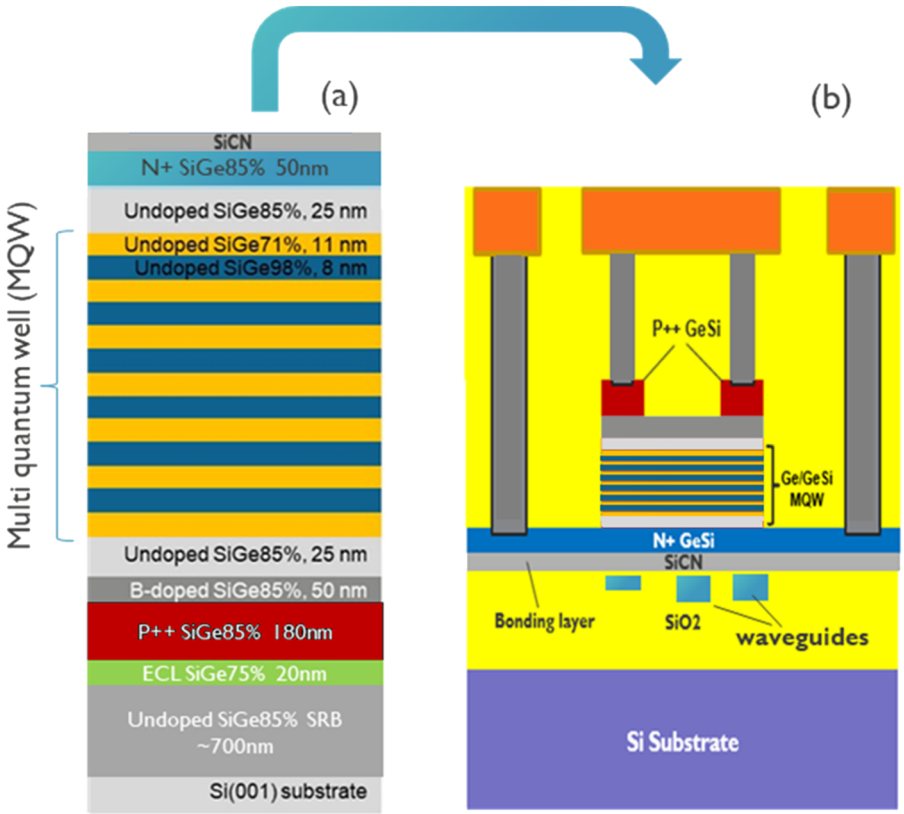

FIG. 1. (a) SiGe 85% QCSE stack with a 700 nm SRB and a 20 nm ECL, (b) schematic of the SiGe QCSE modulator fabricated on a bonded photonic wafer (after bonding, all SiGe layers are flipped and represented as GeSi).

were also done in Lam Research 2300 KiyoGX by using test SiGe wafers after epitaxial growth without bonding.

The SRB layer was removed using a CF_4:SF_6:N_2 chemistry at a ratio of 18:2:9. The etch was performed at a chamber pressure of 3 mTorr, TCP power of 500 W, and bias voltage of 75 V.

B. Transfer matrix method (TMM) modeling

Full-spectrum TMM simulations employed open-access refractive index data (both the real and imaginary components) for SiGe alloys across the wavelength range monitored by the dry etch tool.

The model stack closely approximated the experimental structure shown in Fig. 1(a): 60 nm SRB $Si_{0.20}Ge_{0.80}$/180 nm $Si_{0.20}Ge_{0.80}$/50 nm $Si_{0.20}Ge_{0.80}$/25 nm $Si_{0.20}Ge_{0.80}$/QW-6 × 7 ($Si_{0.28}Ge_{0.72}$/$Si_{0.11}Ge_{0.89}$, 8 nm/11 nm)/25 nm $Si_{0.20}Ge_{0.80}$/50 nm $Si_{0.20}Ge_{0.80}$/50 nm SiC/Si substrate. The Ge content of the modeled SiGe stack differed by ~5% from experimental values (it was 85% Ge in the grown SRB); doping profiles were not explicitly modeled. Refractive index data were sourced from Ref. 10.

Both "as-grown" and "bonded" stack configurations were simulated to match experimental conditions. For each simulation, SRB thickness was adjusted to the measured value, and the ECL was included when present. Wavelength and etch depth sampling intervals ranged from several nanometers (preliminary runs) to sub-nanometer resolution (final simulations). TMM-based simulations generated 3D reflectivity datasets $R(\lambda, d)$ spanning all monitored wavelengths and etch depths.

C. Light spectral reflectometry (LSR)

Making the terminology more general, the term light spectral reflectometer (LSR) in this work denotes a class of *in situ* reflectometry systems that includes differences in illumination source (laser or broadband), source geometry (linear or point), and tool vendor (e.g., Lam Research or others). However, each subclass can also have the same acronym, LSR, as it is commonly found in the literature.[11–13]

As discussed in Refs. 1, 5, and 6, LSR is an active optical metrology system in which an external light source is directed approximately orthogonally toward the wafer surface to monitor reflectivity during plasma etch processing. The LSR used in this study (Lam Research) employs a broadband flash-lamp source that emits microsecond-scale high-intensity pulses over a spectral range of ~200–900 nm, depending on the hardware configuration. To avoid uncertainty associated with extrapolated optical constants, only the portion of this range for which SiGe optical parameters are available in Ref. 10 is used in the analysis.

The coherence length, L_{coh}, of such broadband sources is approximated by $L_{coh} \approx \lambda^2/\Delta\lambda$, where λ is the central wavelength and $\Delta\lambda$ is the full width at half maximum (FWHM) of the source spectrum.

For a source with a Gaussian spectral profile, this expression may be modified by a numerical factor that depends on the specific definitions used for spectral width and coherence length. In many practical implementations, this factor falls below unity, reflecting the more accurate relation between coherence length and the Gaussian spectral envelope.[14,15] If the optical path difference between two reflecting surfaces exceeds L_{coh}, interference fringes wash out and depth resolution is lost. By considering the most typical characteristics of the broadband lamp,[16] the L_{coh} can be estimated to yield values in the low-micrometer range, which is good enough to deal with etch thicknesses of a micrometer range (ideally, film thickness $<L_{coh}/2$) that is applicable to our stacks. Thicker stacks may require either a laser source that has much larger L_{coh}, or a modification of the broadband source to narrow down the $\Delta\lambda$ to increase L_{coh}.

The fastest sampling rate is limited by 100 ms, although the value can be adjusted at the tool level. The sampling interval for wavelength is typically defined by 0.8 nm for the raw reflectivity data accusation in this experiment. The outcome of the experimental run represents a 3D dataset of intensity of reflected light as a function of etching time for the span of wavelengths defined by LSR detection range, i.e., $I(\lambda, t)$. Due to the fact that sampling intervals could be different in experimental and modeling datasets, the closest values of wavelength were used from both datasets to compare results in this paper.

Adapted from Ref. 3 to our case, the field-power representation of the light reflection process is shown in Fig. 2. In our paper, reflectivity and reflectance should be treated as synonyms used to describe the fraction of incident light reflected by a surface, which is usually denoted as R.

D. Reflectometry detection limit

The detection limit is a complex question, which depends on several experimental and physical factors. When the etching starts from a thin film that is exposed directly to plasma etching, the transient stabilization time of both the plasma and the spectrometer may limit the detectable thickness, effectively shifting the detection limit toward thicker films. In our case, the thin delta layer (ECL) is embedded in the "bulk" material. During etching, both the plasma and the spectrometer are already stabilized when the etch front approaches the ECL. It is interesting to estimate the detectable limit of ECL thickness for the experimental configuration used in this paper.

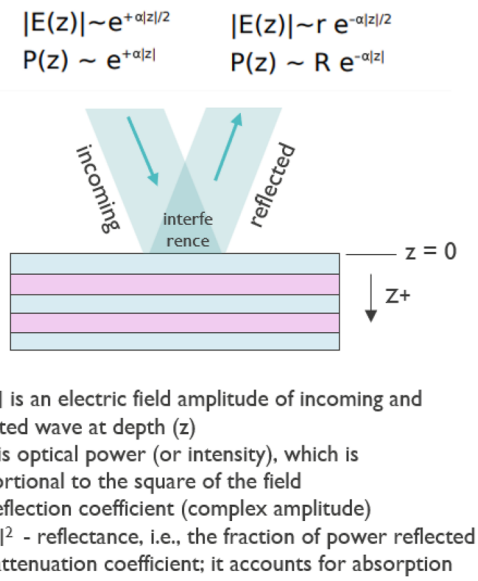

FIG. 2. Field-power representation of light reflection in thin-film multilayer structures.

The refractive index contrast between ECL and surrounding material should differ enough at selected wavelength, which we get by shifting ECL composition by 10% with respect to the SRB. We assume that the sampling rate will not limit the resolution at reduced thickness of ECL, i.e., either the etch rate is slow enough or sampling rate is fast enough to provide at least several measurement points across the minimum ECL thickness.

Compared to ellipsometry, which measures both amplitude and phase changes of polarized light, reflectometry records only the reflected intensity. Although interference effects depend on the optical phase difference between waves, the phase is not measured directly but contributes indirectly through the resulting intensity modulation. The intensity modulation of reflectivity has far lower slope than ellipsometric phase change, so the ellipsometry is typically considered about an order of magnitude more sensitive than reflectometry for ultra-thin films, such as SiGe. As a result, while advanced ellipsometers can achieve sub-nanometer thickness sensitivity under favorable conditions, the practical detection limit for reflectometry is expected to lie in the single-nanometer range.

Experimentally, we know that the selected 20 nm ECL is working quite well. Moreover, the experimental and modeling results shown in Fig. 3 and discussed later in this paper demonstrate that QW layers with thicknesses of ~8 to 11 nm can be clearly resolved by reflectometer at a probing wavelength around 500 nm. Therefore, if the sampling rate is not the limiting factor, the ultimate detection limit of reflectometry should be smaller than these values.

We consider a multilayer stack containing an embedded ECL layer of thickness d. The objective is to estimate the theoretical minimum detectable thickness, $d_{\min}$, at which the layer can be identified by reflectometry. In contrast to modeling, the real-world measurement noise pushes limits toward higher side, i.e., sets the limit on detectability, which can be estimated by using a common metric of minimal detectable thickness, $d_{\min}$, for reflectometry,

$$d_{\min} \approx \frac{1}{S_R}\sigma,$$

where $S_R = \frac{\partial R}{\partial d}$ is the reflectometry sensitivity and σ is the instrument noise.

Thus, the maximum possible sensitivity is near the inflection of the interference fringes. When the ECL is reached during SRB etching, absorption can be treated as constant, and the reflectivity oscillations are approximated by a cosine function.

For films much thinner than the probing wavelength, reflectivity varies as

$$R(d) \approx R_0 + A\cos\left(\frac{4\pi nd}{\lambda}\right),$$

where A is the fringe modulation amplitude, R_0 is the background reflectivity of the structure, and d is the film thickness.

So, the slope is

$$\frac{\partial R}{\partial d} \approx -A\left(\frac{4\pi n}{\lambda}\right)\sin\left(\frac{4\pi nd}{\lambda}\right).$$

The maximum slope occurs when the sine term is equal ±1,

$$\max\left|\frac{\partial R}{\partial d}\right| = \frac{4\pi nA}{\lambda}.$$

Thus,

$$d_{\min} \approx \frac{\sigma\lambda}{4\pi nA}.$$

The above expression represents an optimistic estimate of the detection limit. In practice, the minimum detectable thickness shifts toward larger values in regions where $\partial R/\partial d$ is smaller than its maximum value. In Sec. III, the formula is going to be populated with experimental parameters to estimate the practical detection limit of the experimental setup.

III. RESULTS AND DISCUSSION

A. Agreement between TMM and experimental data

As shown for Ge-rich stack, TMM simulations exhibit excellent agreement with experimental LSR data (Fig. 3) despite ~5% Ge composition differences and omitted doping profiles. The quantum-well spectral response peaks at 500 ± 50 nm for the Ge-rich stack ($Si_{0.20}Ge_{0.80}$), while the Si-rich analog ($Si_{0.80}Ge_{0.20}$) exhibits a blue-shifted QW-sensitive region. This wavelength sensitivity region validates the stack composition near 85% Ge for Ge-rich sample and identifies optimal wavelengths for ECL-based end point detection (discussed below).

B. End point detection without ECL

First set of wafers had a stack without ECL with SRB thickness ~600 nm. If other layers besides SRB have a limited thickness variability because of a good epitaxial process control, it is possible to rely upon the overall stack thickness in-between SRB and bonding layer of SiCN. To stop the SiGe SRB etching at certain depths above the bonding interface layer, e.g., at 600 nm, one should shift from the QW-sensitive spectral region to longer wavelengths. The goal is to identify wavelength combinations and their functions that produce a distinct signal at the desired depth during SRB etch-back of QCSE stack. However, we must limit the wide variety of possible mathematical functions that could potentially be used by selecting a combination of several intensities and their derivatives, which makes such end point algorithm function applicable on our dry etch tool. In dry etch tool end point definition, one typically records a band of a certain width rather than an intensity of a separate line. The selected 5 nm bandwidth represents a compromise between noise suppression and preservation of interference contrast. A significantly wider band would smear spectral features, whereas a narrower band would increase noise without substantial benefit in spectral selectivity.

Figure 4 illustrates such approach, showing the selected combo of wavelengths with bandwidth of 5 nm that yields a clear peak at depth of ~600 nm tested by using TMM-generated data. Although simulated data are noise-free, there is a low-pass (LP) filter that has been added to cope with real noisy data. Thus, the suggested end point function consists of an LP filter applied to the ratio of several intensities and their derivatives, as shown in Fig. 4. Meanwhile, due to a certain noise level present in the real spectra, such approach will still require multiple iterations to find a working regime in practice.

C. End point detection with ECL and outlook

The situation can be further simplified if a thin ECL (e.g., ΔGe ≈ 10%) could be added after SRB during "direct" stack growth. For

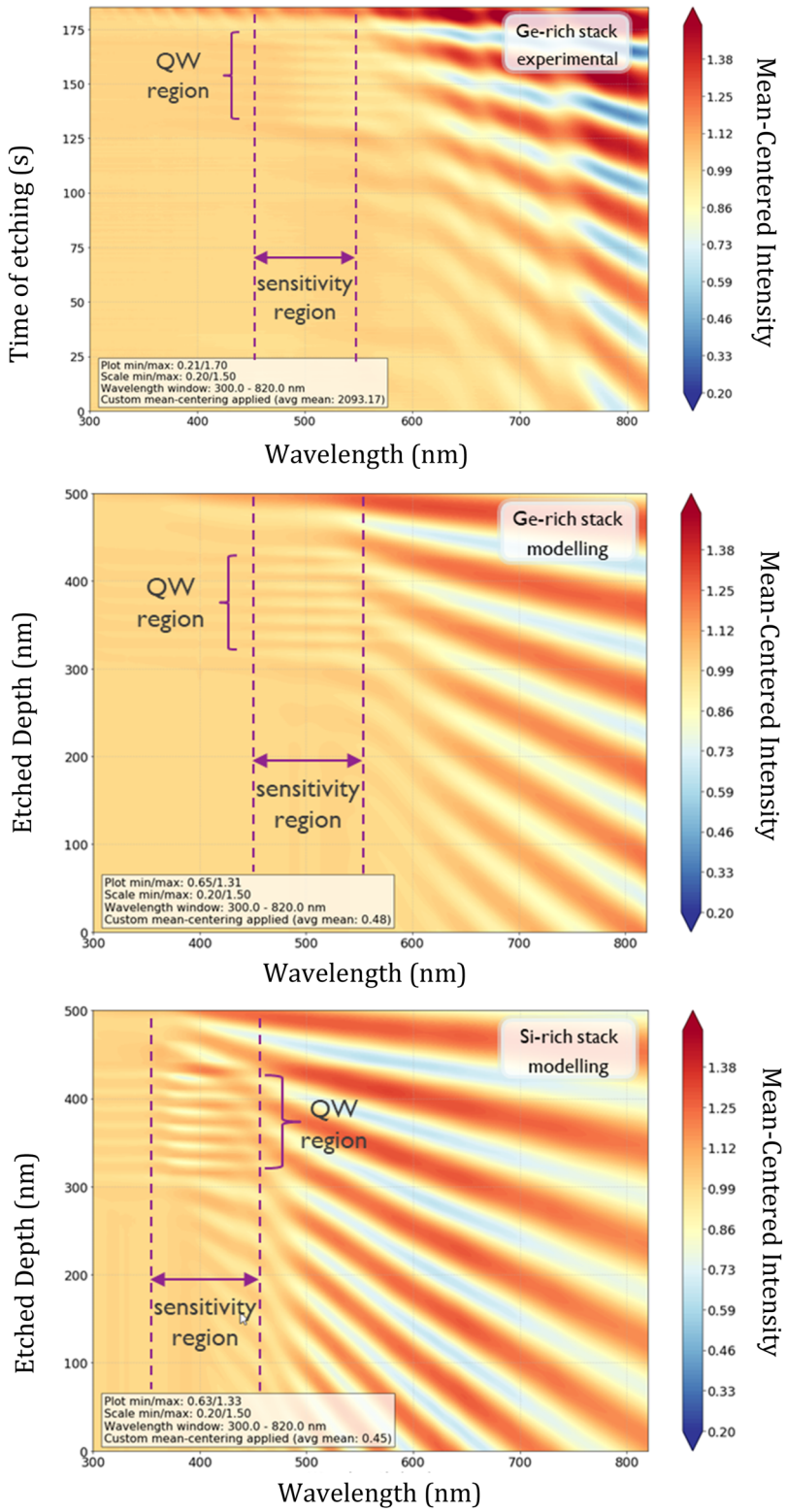

FIG. 3. Comparison of experimental LSR data and TMM simulations for both Ge-rich (SiGe 80%) and Si-rich (SiGe 20%) mimic stacks. The full reflectivity spectrum is shown for the entire QCSE stack etch. The intensities were mean-centered to facilitate comparison. The 60 nm SRB mimic stack is described in Sec. II A.

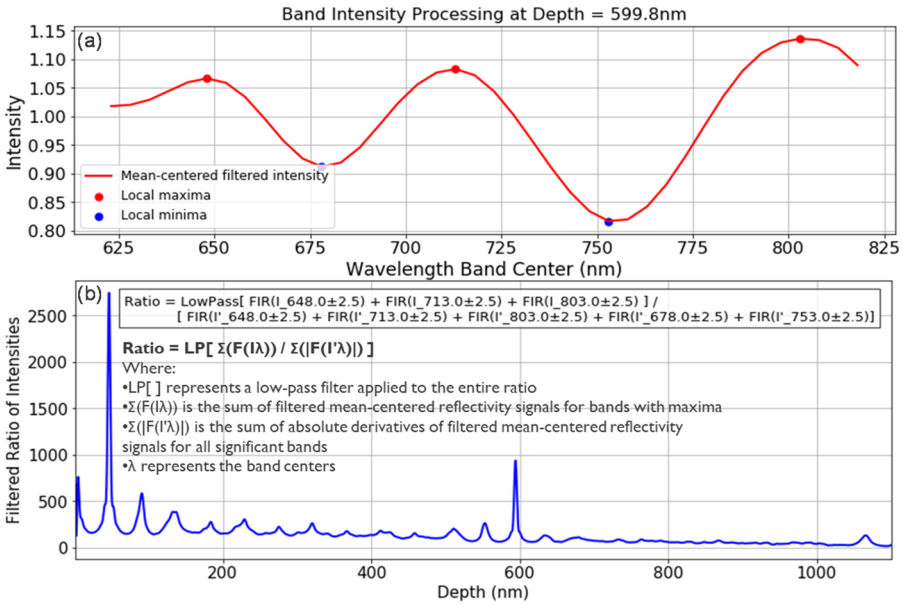

FIG. 4. (a) Extrema points of normalized reflectivity at approximately the targeted etch depth. (b) Combined signal suitable for end point detection at a depth of ~600 nm for the stack without ECL, as suggested by TMM simulations.

example, insertion of a thin SiGe75% ECL [see in Fig. 1(b)] strongly modulates the reflectivity signal at 520 nm, which simplifies the end point definition for the case of SRB etch back step. Both graphs of Fig. 5 clearly show the reflectivity signature of the 20 nm ECL at 520 nm, which lies within the QW sensitivity region of Ge-rich stack identified in Fig. 3. Three other wavelengths, which are shown in Fig. 5 for comparison, are clearly less suitable for robust ECL-based end point setup. By doing TMM modeling, one can plot an overlay of reflectivity for selected wavelength with the actual stack that is shown in the background of Fig. 5 for both "direct" and "flipped" stacks. Such plot allows revealing exact moment when end point should be triggered. Thus, if we want to stop exactly in ECL, we should not trigger at local maximum of the green curve (wavelength of 520 nm) when approaching ECL, but rather at minimum. This is true for both stacks shown in Figs. 5(a) and 5(b).

While we have demonstrated the use of a 20 nm thick ECL layer, it is instructive to estimate the minimum ECL thickness detectable under the present experimental configuration using the expression derived in Sec. II D.

Since the reflectivity is proportional to the normalized detected intensity,

$$R \propto I,$$

the relative noise level in reflectivity can be estimated from the raw experimental intensity–time data (corresponding mean-centered values are shown in Fig. 3) by analyzing the dataset around 520 nm. Considering the mean intensity of a flat region $\bar{I} \approx 3216$ a.u. and the corresponding standard deviation $\sigma_I \approx 10.6$ a.u., the relative instrumental noise level can be estimated as

$$\sigma = \frac{\sigma_I}{\bar{I}} \approx 3.3 \times 10^{-3} \ (0.33\%).$$

The fringe modulation amplitude A can be estimated from the green curve of the flipped stack shown in Fig. 3(b). In the highlighted interval corresponding to etching through the 20 nm ECL, a clear extremum appears. From its amplitude relative to the background, we estimate that $A \leq 0.04$.

Using these parameters in the expression for the minimum detectable thickness gives the limit,

$$d_{\min} > \frac{3.3 \times 10^{-3} \times 520}{4\pi \times 4.5 \times 0.04} \approx 0.8 \ \text{nm}.$$

Considering that the above relation represents an optimistic estimate obtained for the maximum slope of the interference fringe, the practical detection limit is expected to be on the order of ~1 nm under the present experimental conditions.

By focusing on the 520 nm line, which appears to be one of the best for the ECL-based end point definition of given stack, Fig. 6 shows a comparison between experimental and modeling data for a 600 nm SRB stack. As one can see, the overall correlation looks very good although there are a few small discrepancies visible in the spectral lines. Thus, in between QW region and ECL, there is an extra feature present in the experimental LSR spectrum, which is not present in the TMM one. It should be attributed to a doped layer, so this discrepancy is explained by the fact that there was no doping information included in the TMM modeling at this stage. In addition, if we want to have a good peak position overlapping of both spectra shown in Fig. 6, there is some stretching or squeezing required to be done along time axis to get all major peaks matched. These observed discrepancies originate not only from the absence of doping-dependent optical constants in the model but also from a 5% compositional offset between the modeled and actual stacks. Since the SiGe etch rate depends on both Ge composition and dopant concentration,[17,18] the experimental structure inherently includes variations that are not explicitly incorporated into the current TMM implementation. As a result, small residual differences between simulated and measured spectra are expected.

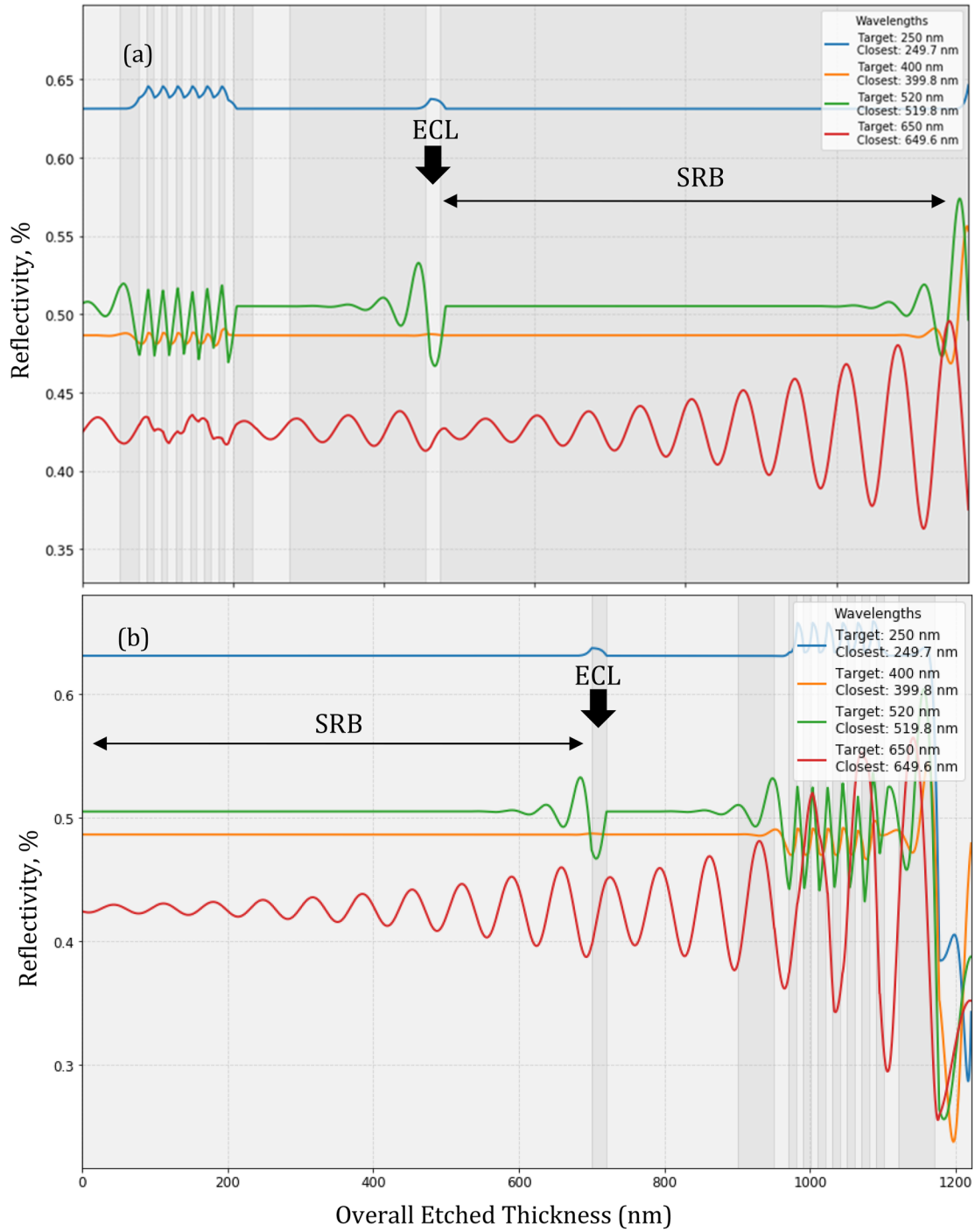

FIG. 5. TMM simulation of QCSE stack with stack overlay: (a) As-grown "direct" stack with 700 nm SRB and 20 nm ECL. (b) Bonded "flipped" stack configuration with the same layer composition.

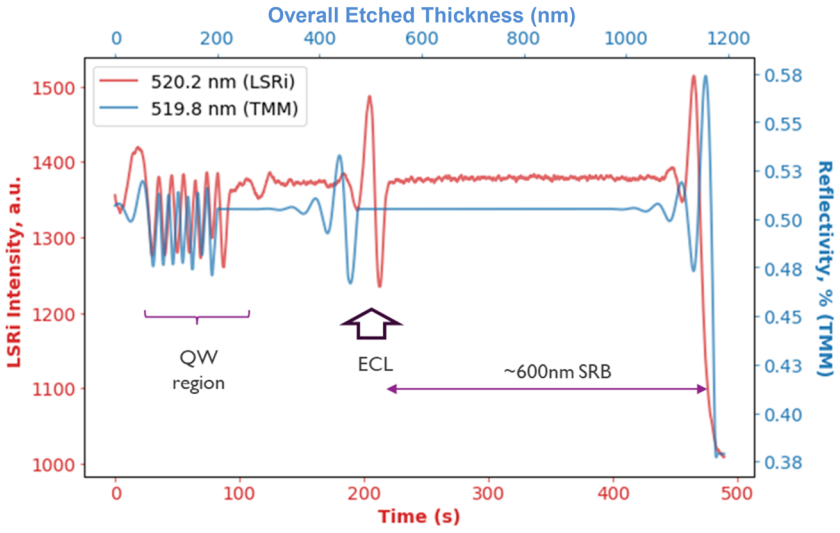

FIG. 6. Comparison of TMM simulation and LSRi measurements at a wavelength of ~520 nm for the "direct" QCSE stack etch, comprising a 600 nm SRB and 20 nm ECL layer (SiGe 72%). LSRi of Lam Research is an integrated version of the reflectometer that has a simplified design compared to LSR, but its working principle stays the same.

After eliminating all the identified offsets, future work may employ the dynamic time warping (DTW) technique [previously demonstrated in reactive ion etching (RIE)[1]] to quantify etch rate variations among differently doped QCSE layers based on LSR spectra and TMM modeling.

IV. CONCLUSION

In this work, we have demonstrated the use of TMM modeling to describe light spectral reflectivity datasets and to control plasma etching in SiGe-based photonic device fabrication, achieving near-perfect agreement between simulated and experimental LSR spectra. The small remaining offsets are attributed to the use of a mimic SiGe stack in the simulations, whose Ge composition and doping levels differ slightly from those of the experimental QCSE modulator structure. The practical applicability of the method was validated through end point characterization of the SiGe SRB etch-back step, both with and without the etch-contrast layer (ECL). The approach is readily adaptable to other multilayer systems. Future extensions of this approach may include incorporating patterned-wafer topography into the reflectivity simulations to further enhance predictive capability.

ACKNOWLEDGMENTS

The authors thank the NanoIC pilot line for supporting this initiative.

AUTHOR DECLARATIONS

Conflict of Interest

The authors have no conflicts to disclose.

Author Contributions

A. P. Milenin: Conceptualization (lead); Data curation (lead); Formal analysis (lead); Methodology (lead); Software (lead); Visualization (lead); Writing – original draft (lead); Writing – review & editing (lead). **J. R. Vaskasi**: Data curation (supporting); Formal analysis (supporting); Resources (supporting). **D. Kazakov**: Data curation (supporting); Software (supporting); Visualization (supporting). **Y. Shimura**: Project administration (supporting); Resources (equal). **I. G. Koo**: Funding acquisition (equal); Project administration (supporting); Resources (equal). **F. Ferraro**: Funding acquisition (equal); Project administration (equal). **K. Devriendt**: Funding acquisition (equal); Project administration (equal); Resources (equal).

DATA AVAILABILITY

The data that support the findings of this study are available from the corresponding author upon reasonable request.

REFERENCES

[1] A. P. Milenin, B. T. Chan, and F. Lazzarino, "Assessment of STI dry etch process variability by means of dynamic time warping technique," Jpn. J. Appl. Phys. **62**, SI1004 (2023).
[2] T. G. Mackay and A. Lakhtakia, *The Transfer-Matrix Method in Electromagnetics and Optics* (Springer, 2020).
[3] S. J. Byrnes, "Multilayer optical calculations," arXiv:1603.02720 (2016).
[4] A. Luce, A. Mahdavi, F. Marquardt *et al.*, "TMM-fast: A transfer matrix computation package for multilayer thin-film optimization," arXiv:2111.13667 (2021).
[5] P. A. Heimann and R. J. Schutz, "Optical etch-rate monitoring: Computer simulation of reflectance," J. Electrochem. Soc. **131**, 881–885 (1984).
[6] V. C. Venugopal and A. J. Perry, "Reflectometry-based approaches for in-situ monitoring of etch depths in plasma etching processes," Proc. SPIE **4779**, 98–107 (2002).
[7] P. Chaisakul, V. Vakarin *et al.*, "Recent progress on Ge/SiGe quantum well optical modulators, detectors, and emitters for optical interconnects," Photonics **6**(1), 24 (2019).
[8] A. Kandeel *et al.*, "64 Gb/s O-band GeSi quantum-confined Stark effect electroabsorption modulators integrated in a 300 mm silicon photonics platform," J. Lightwave Technol. **43**, 2794–2802 (2025).
[9] Y.-H. Kuo, H.-W. Chen, and J. E. Bowers, "High speed hybrid silicon evanescent electroabsorption modulator," Opt. Express **16**(13), 9936–9941 (2008).

[10]M. Polyanskiy, RefractiveIndex.INFO: Refractive index database (2022); http://refractiveindex.info.
[11]M. Lee, J. Park, and J. Kim, "Line spectroscopic reflectometry for rapid and large-area thickness measurement," Opt. Express **31**(20), 32241–32252 (2023).
[12]M. Lee, J. Park, and J. Kim, "Line spectral reflectometry for high-speed, large-area thickness measurement," in *2024 Conference on Lasers and Electro-Optics—Pacific Rim (CLEO-PR)*, *Technical Digest Series* (Optica Publishing Group, 2024), p. Th1E_3.
[13]S. N. M. Mestanza and N. C. Frateschi, "Laser reflectometry *in situ* monitoring structural and growth effects on the electron cyclotron resonance etching of $In_{0.49}Ga_{0.51}P$ layers in Al-free laser structures," J. Vac. Sci. Technol. B **19**, 192–196 (2001).
[14]S. Dahiya, A. Tyagi, A. Mandal, T. Pfeifer, and K. P. Singh, "Ultrathin picoscale white light interferometer," Sci. Rep. **12**, 8656 (2022).
[15]P. Jansz, S. Richardson, G. Wild, and S. Hinckley, "Modeling of low coherence interferometry using broadband multi-Gaussian light sources," Photonic Sens. **2**, 247–258 (2012).
[16]J. H. Goncz, "The xenon flash lamp as a light source for spectroscopy," Appl. Spectrosc. **20**, 289–295 (1966).
[17]S. N. R. Kazmi *et al.*, "Deep reactive ion etching of in situ boron doped $Ge_{0.7}Si_{0.3}$ using SF_6 and O_2 plasma," Microelectron. Eng. **110**, 311–314 (2013).
[18]C. Li, H. Lin, J. Li *et al.*, "Growth and selective etch of phosphorus-doped silicon/silicon–germanium multilayers structures for vertical transistors application," Nanoscale Res. Lett. **15**, 225 (2020).